NATIONAL INSTITUTE FOR OCCUPATIONAL SAFETY AND HEALTH

NTRC NANOTECHNOLOGY RESEARCH CENTER

Generation and characterization of aerosolized particles from nanoclay-enabled composites during sanding

EG Lee[1], L Cena[2], J Kwon[3], A Afshari[1], HD Park[3], A Wagner[4], S Agarwhal[4], R Gupta[4], G Casuccio[5], K Bunker[5], T Lersch[5], S Friend[1], TA Stueckle[1],

[1] HELD, NIOSH, Morgantown, WV; [2] West Chester University, PA; [3] KOSHA, S. Korea; [4] Chemical and Biomedical Engineering, West Virginia University, Morgantown, WV;

[5] RJ Lee Group, Monroeville, PA

Abstract# 1105

Motivation and Purpose

Nanoclay-enabled nanocomposites continue to rapidly grow in novel applications including food and beverage packaging, biomedical tools, fire retardants, automobile/aerospace parts industry, etc. Previous studies have found adverse toxicological effects due to the exposures to raw nanoclay materials, including pulmonary health effects (e.g., respiratory tract irritation), hemolysis, cytotoxicity effects (e.g., decreased cellular proliferation), mitochondrial and membrane damage, reactive oxygen species generation, and genotoxic effects. Manufacturing, use, machining, and disposal of nanocomposites used in those applications could lead to the potential release of aerosolized particulate including intact nanocomposite, nanocomposite with surface nanoclay protrusions, or free release of nanoclay particles from the polymer matrix. Occupational exposures to airborne nanocomposites are expected in increase in the near future, but are poorly understood.

The objective of this study was to simulate industrial sanding of nanoclay-embedded polypropylene composites and to characterize particles generated to estimate occupational exposure levels.

Methods and Materials

Nanoclay-enabled polypropylene nanocomposite synthesis: Polypropylene (PP; Amoco BP 1246) was selected as a model virgin thermoplastic material. Two types of nanoclay, Cloisite® 25A and Cloisite® 93A (Southern Clay Products, Gonzalez, TX) at 1% and 4% of concentration by weight, were embedded into the PP via melt mixing and thermal compression molding using a metal frame built in-house. Virgin PP (0% nanoclay) served as a comparative control of non-ENM-enabled thermoplastic composite (Fig.1).

Virgin PP | 1% Clois93A | 4% Clois93A | 1% Clois25A | 4% Clois25A

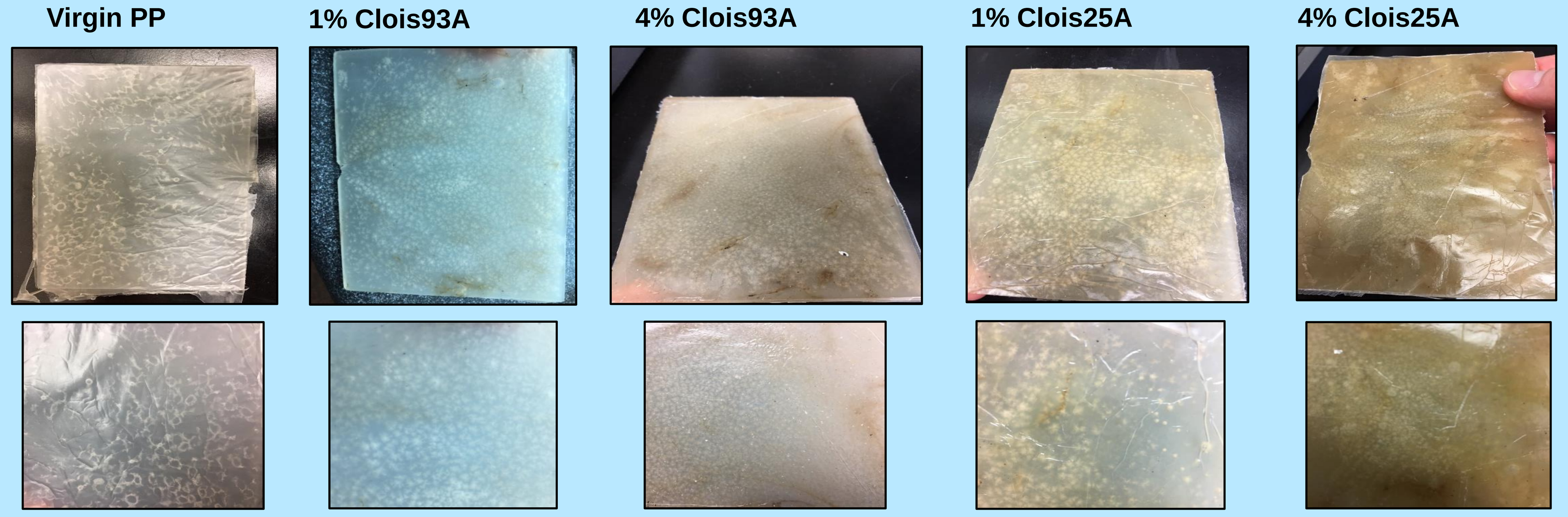

Fig. 1 Representative images of bulk ONC-enabled PP nanocomposites.

Characterization of mechanical properties: Mechanical properties including Young's modulus, tensile strength, toughness, and elongation at break were determined using an Instron E1000 under a 2 kN load cell. Toughness was then calculated by integrating the area under stress by strain curve. Crystallinity and degree of nanoclay dispersion of each composite was determined with a PANalytical X'Pert Pro and a Bruker D8 Discovery XRDs. Visualization of dispersed nanoclay within the PP matrix was also performed via TEM analysis.

Controlled Machining of Nanocomposite: Sanding particles of nanocomposites and virgin materials were generated using an automated, controlled exposure chamber (Fig. 2). Two types of sandpaper (ZrAlO and SiC) and two grit sizes (P100 and P180) were studies. CPC, SMPS, APS, MOUDI impactor, and IOM samplers were deployed to analyze particle release real-time and for post-machining analyses. Temperature was also monitored during sanding.

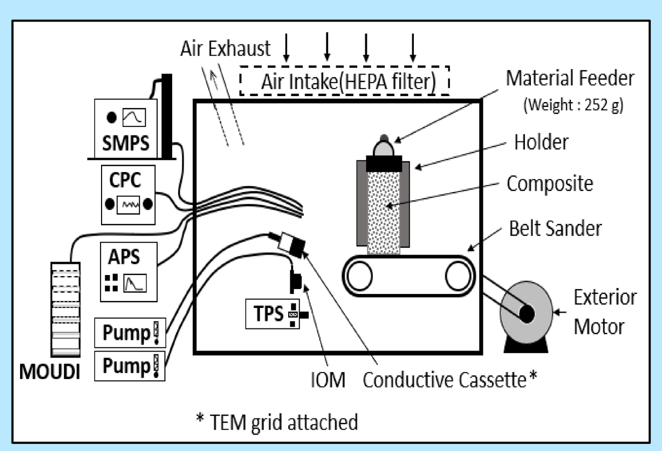

Fig. 2. Sanding chamber apparatus to measure and collect released particulate in real-time.

Electron Microscopy Analysis: Computer-controlled scanning electron microscopy (CCSEM) analysis coupled with EDS was conducted on collected Inhalable size fraction filters by RJ Lee Group to determine number, mass, size, and chemistry characterization of generated dusts. FESEM images and EDS of the individual particles ≥ 1 μm were captured during the CCSEM analysis using IntelliSEM software (about 3000-5000 particles per each material). Criteria were developed to sort composite and sandpaper particles based on our preliminary work comparing particles' morphology and elemental compositions. ONC protrusions were identified and quantified by evaluating > 200 particles per sample.

Characterization of bulk nanoclay composite

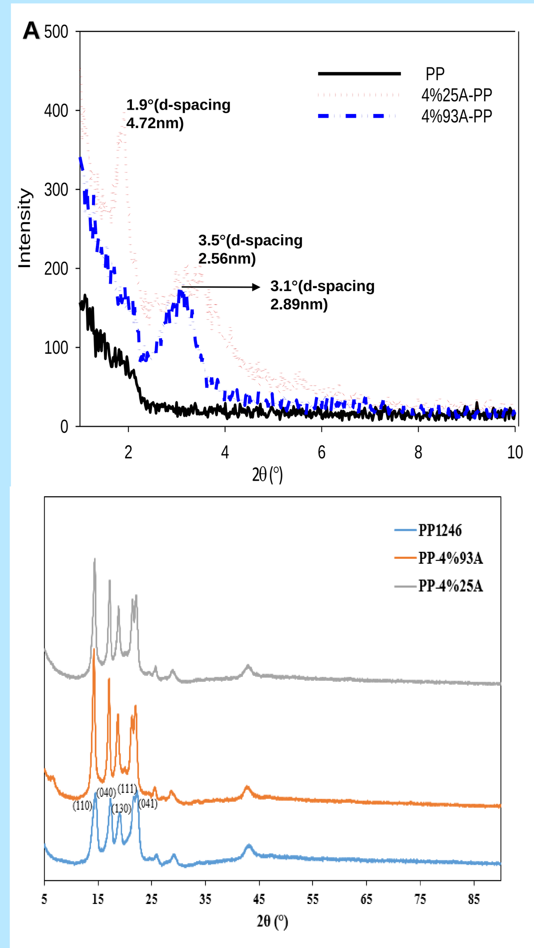

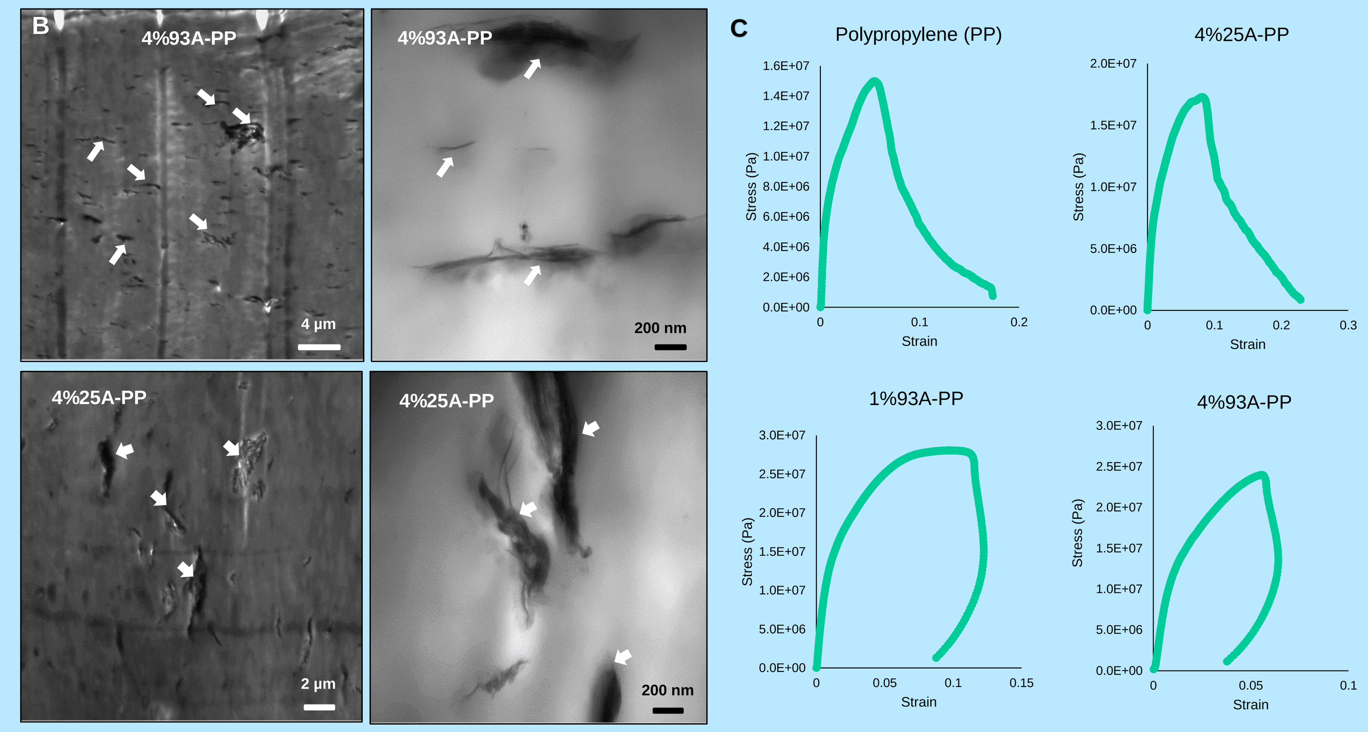

Fig. 3. Dispersion characteristic of nanoclay-enabled PP composites compared to virgin PP determined via (A) X-ray diffraction and (B) TEM images showing spacing of nanoclay platelets (white arrows) within the PP matrix and crystallinity of the nanocomposite. (C) Representative stress vs. strain curves for composites. Exfoliated and intercalated nanoclay did not change PP matrix structure, but did alter strength characteristics.

Abrasion Real Time Particle Release Assessment

Table 1. Summary of mechanical properties

Material ID	Composites	Sand paper grit	Tensile Strength (SE) (MPa)	Elongation at break (SE) (mm)	Toughness (SE) (J m^{-3})	Young's Modulus (SE) (Gpa)
PP	Polypropylene (PP) (virgin)	P100 P180	18.1 (2.2)	4.5 (1.1)	324020 (78252)	1.32 (0.09)
1%25A-PP	Cloisite 25A-PP (1% w/w)	P100 P180	28.2 (0.8)	3.8 (0.4)	620149 (39378)	1.13 (0.05)
4%25A-PP	Cloisite 25A-PP (4% w/w)	P100 P180	13.7 (1.7)	8.0 (1.1)	318351 (85147)	0.88 (0.07)
1%93A-PP	Cloisite 93A-PP (1% w/w)	P100 P180	26.0 (1.0)	5.3 (0.9)	670356 (85117)	1.28 (0.06)
4%93A-PP	Cloisite 93A-PP (4% w/w)	P100 P180	24.4 (0.5)	3.7 (0.9)	448494 (42599)	1.45 (0.09)

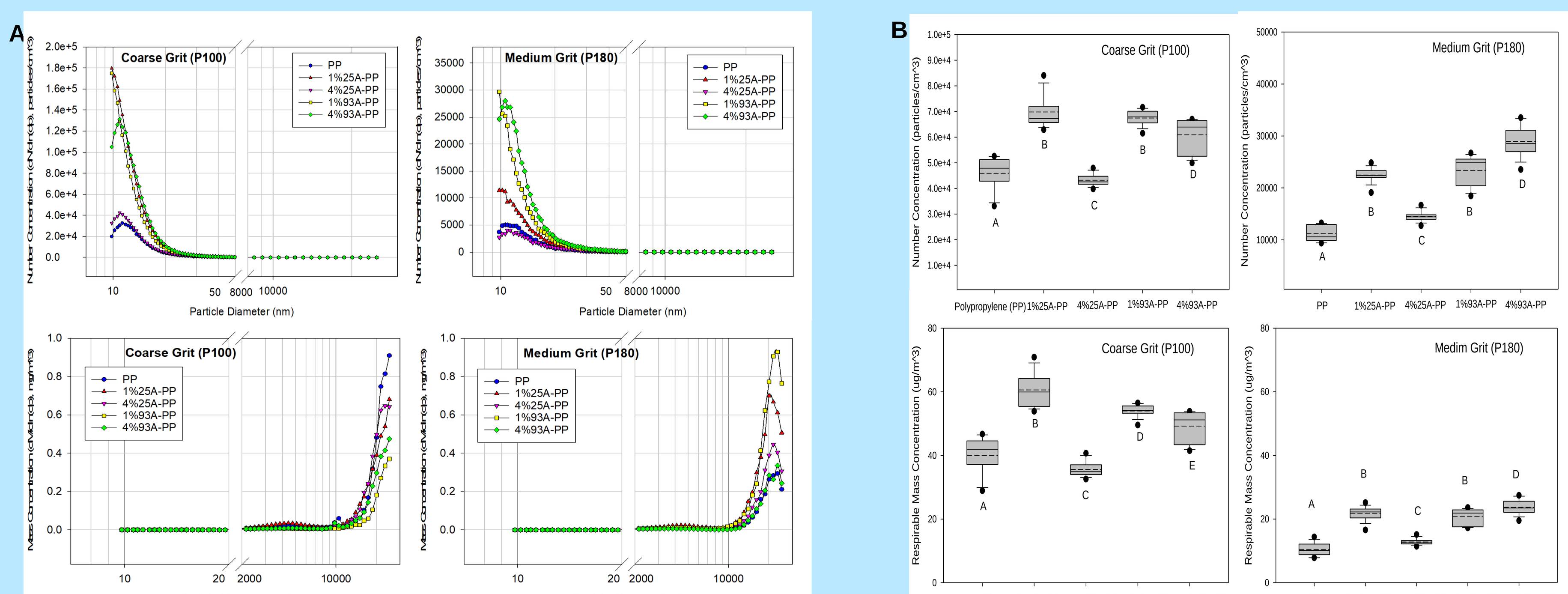

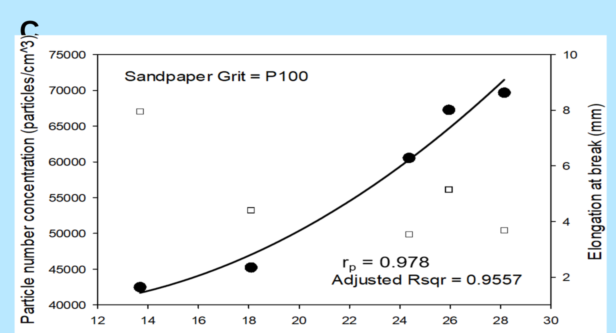

Fig. 4. Characterization of dusts released during sanding of ONC-enabled polypropylene nanocomposite. A) Comparison of particle size distributions by number (upper) and mass (lower) concentrations from DRIs. B) Particle number concentrations (top row) and respirable mass concentrations (bottom row) by sandpaper type. Different letters indicate statistically significant differences (p-value < 0.05). C) Relationship of tensile strength with particle number concentrations (solid circles) and elongation at break (open squares).

Computer controlled Scanning FESEM / EDS Quantification of Particulate

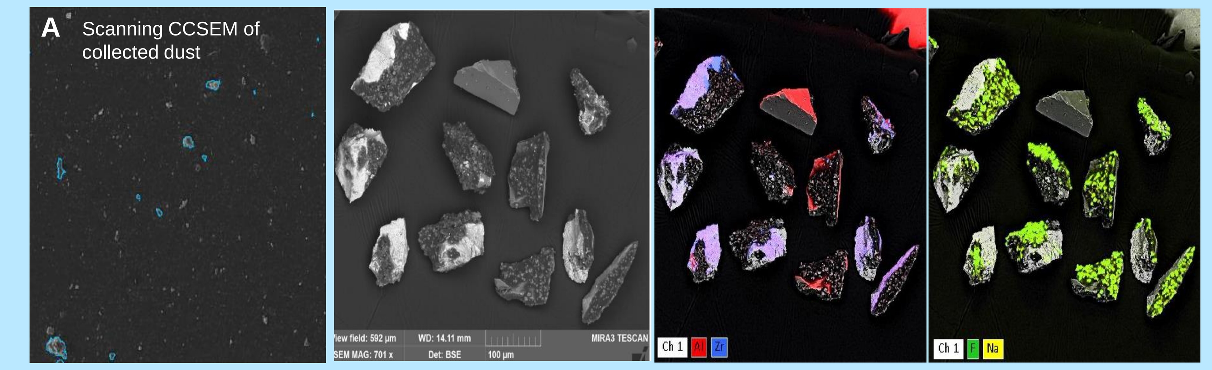

B	Number percent (%)						Weight percent (%)					
	Compo-site[a]	Al-Zr	Ca-rich	C-rich	Na-F-Al	Other[b]	Compo-site[a]	Al-Zr	Ca-rich	C-rich	Na-F-Al	Other[b]
Sandpaper	N/A	11	8.6	36	23	21	N/A	22	5.1	18	25	30
PP	11	1.4	43	12	14	19	71	0.6	7.8	15	0.6	5.1
1%25A-PP	2.4	0.5	39	40	8.2	10	17	0.7	22	52	1.4	6.9
4%25A-PP	2.5	0.7	30	46	8.0	13	83	0	4.0	11	0.2	1.8
1%93A-PP	1.9	1.1	39	39	8.6	10	69	0.2	14	14	1.0	1.8
4%93A-PP	2.9	1.7	49	19	13	14	66	0.5	17	11	1.0	4.5

[a] no composition reported due to high C and O signature with trace amounts of Al and Si
[b] includes Al-rich, Zr-rich, C(NaF), Si-Al, Si-Ca, Si-rich, Fe-rich, and miscellaneous

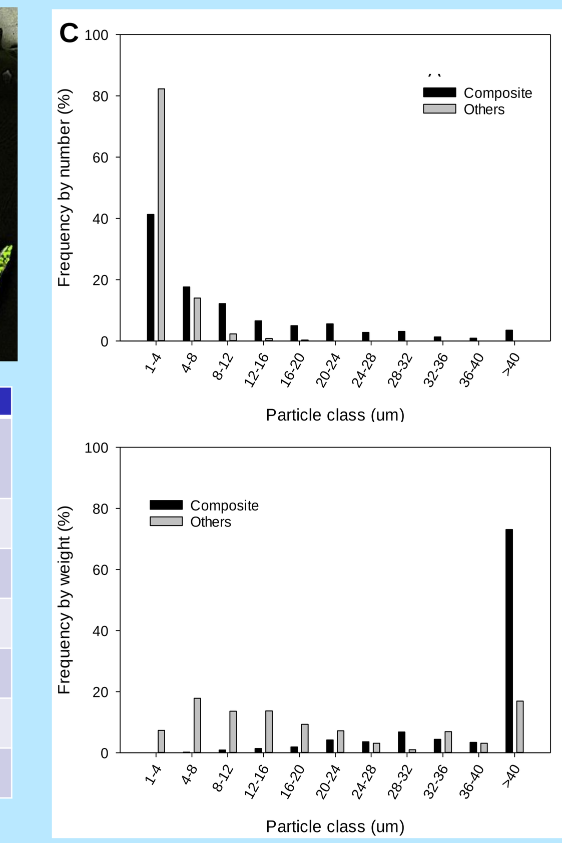

D Material type	Total particles analyzed	Particles per area (P cm^{-2})	Composite particles	Composite particles per area (P cm^{-2})	Composite particles relocated for protrusion examination	Particles with protrusions	Percent of composite particles with protrusions
1%25A-PP	3950	1.6E+04	209	3.91E+02	209	37	18%
4%25A-PP	4049	1.1E+05	214	2.62E+03	214	126	59%
1%93A-PP	4912	2.1E+05	234	4.05E+03	200	66	33%
4%93A-PP	3059	1.1E+05	202	3.31E+03	202	54	27%

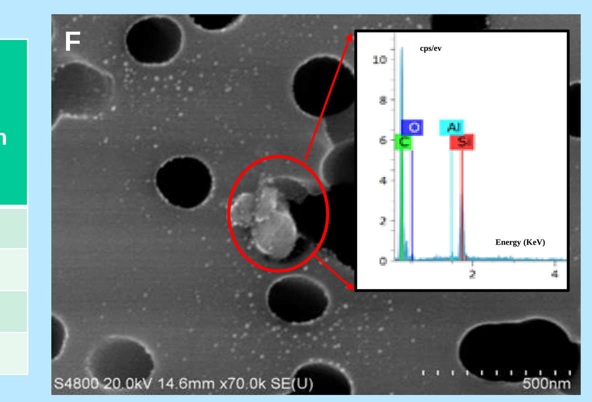

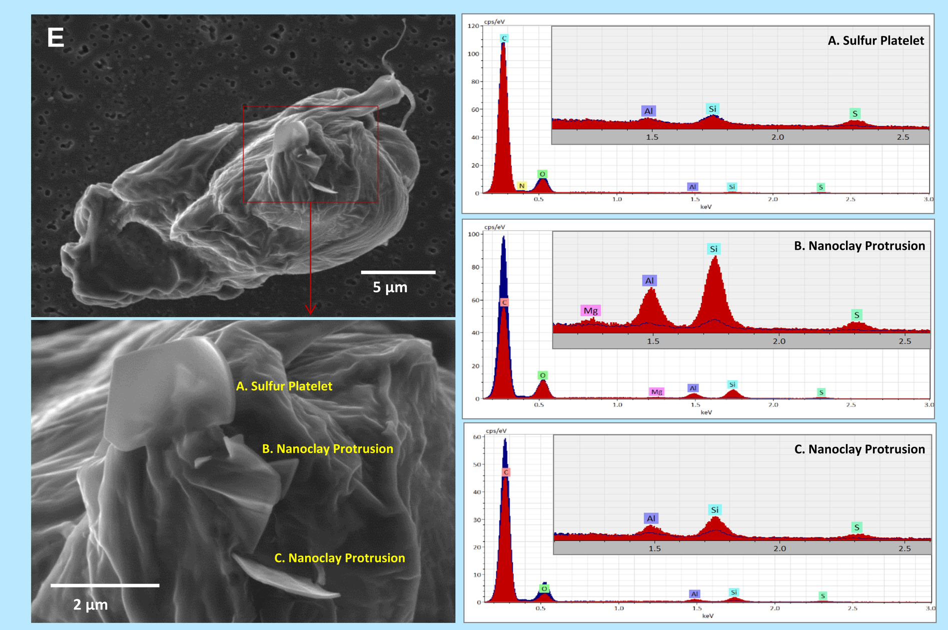

Fig. 5. Quantitative CCSEM/EDX analysis of collected airborne dust (≥1 μm) from sanding of ONC-enabled nanocomposite. A) Filter scanning and X-ray elemental mapping of composite dusts and sandpaper particulate. B) Summary of particle analysis by number and weight percent (particles ≥ 1 μm; P100 sandpaper). C) Size distribution frequency by number (upper) and weight (lower) for 4%93A-PP. D) Quantitative assessment of nanoclay protrusions from ONC-enabled PP nanocomposite. E) Secondary electron images and EDS of a sanding composite particle with protrusions (4%93A-PP). The composite particle EDS (blue) and protrusion/platelet EDS (red) overlays distinguish EDS counts related to platelet features from the composite particle background counts. F) Submicron platelet-shaped aluminosilicate particle from sanding of 1% Clois25A PP nanocomposite indicating potential for 'free release' of nanoclay from PP matrix, but this was a rare occurrence.

Conclusions

- Airborne particle release during machining of ONC-enabled polypropylene nanocomposite depended on coating type, percent ONC load, ONC dispersion within the matrix, and sandpaper grit size. These factors impacted nanocomposite tensile strength, toughness, and elasticity.
- Nanocomposites with 1% ONC loading resulted in 69,000 particles / cm^3 during machining, regardless of coating type followed by 4% Clois93A which showed improved dispersion compared to 4% Clois25A. Both 1% nanocomposites showed a shift from large inhalable fraction towards increased counts in the ultrafine particle fraction compared to 4% and virgin composites. Tensile strength of each nanocomposite was highly correlated with airborne particle concentration.
- Collected airborne dust particulate (≥1 μm) was a complex mixture comprised of nanocomposite particles and sandpaper particles, diverse in elemental composition. Nanocomposite particles dominated the percent mass released for most nanocomposites while calcium-rich and carbon-rich non-composite particles dominated percent number released.
- 22-55% of nanocomposite particles had ONC protrusions out of the PP matrix with the remainder of composite possessing detectable levels of ONC embedded in the matrix. Limited analysis of ultrafine particulate suggested that free release of ultrafine aluminosilicate particles (i.e. nanoclay) was rare.